

PAPER • OPEN ACCESS

Neutron transfer in reaction $^{18}\text{O} + ^{181}\text{Ta}$ with formation of neutron-rich oxygen isotopes

To cite this article: Yu E Penionzhkevich *et al* 2020 *J. Phys.: Conf. Ser.* **1555** 012031

View the [article online](#) for updates and enhancements.

You may also like

- [Effect of positive Q-value neutron transfers on sub-barrier fusion reactions](#)
Pei-Wei Wen, , Zhao-Qing Feng *et al.*
- [Cooper pair transfer in nuclei](#)
G Potel, A Idini, F Barranco *et al.*
- [The Impact of Neutron Transfer Reactions on the Heating and Cooling of Accreted Neutron Star Crusts](#)
H. Schatz, Z. Meisel, E. F. Brown *et al.*



The Electrochemical Society
Advancing solid state & electrochemical science & technology

242nd ECS Meeting

Oct 9 – 13, 2022 • Atlanta, GA, US

Early hotel & registration pricing
ends September 12

Presenting more than 2,400
technical abstracts in 50 symposia

The meeting for industry & researchers in

BATTERIES
ENERGY TECHNOLOGY
SENSORS AND MORE!



Register now!



ECS Plenary Lecture featuring
M. Stanley Whittingham,
Binghamton University
Nobel Laureate –
2019 Nobel Prize in Chemistry



Neutron transfer in reaction $^{18}\text{O} + ^{181}\text{Ta}$ with formation of neutron-rich oxygen isotopes

Yu E Penionzhkevich^{1,2}, S M Lukyanov¹, A K Azhibekov^{1,3,4},
M A Naumenko¹, T Issatayev^{1,3,4}, I V Kolesov¹, V A Maslov¹,
K Mendibayev^{1,3,4}, V A Zernyshkin¹, K A Kuterbekov³,
A M Mukhambetzhan⁵

¹ Flerov Laboratory of Nuclear Reactions, Joint Institute for Nuclear Research, Dubna, Moscow Region, 141980, Russian Federation

² Department of Experimental Methods in Nuclear Physics, National Research Nuclear University MEPhI, Moscow, 115409, Russian Federation

³ L N Gumilyov Eurasian National University, Nur-Sultan, 010000, Kazakhstan

⁴ Institute of Nuclear Physics, Ministry of Energy of Republic of Kazakhstan, Almaty, 050032, Kazakhstan

⁵ Korkyt Ata State University, Kyzylorda, 120001, Kazakhstan

E-mail: anaumenko@jinr.ru

Abstract. Differential cross sections for the formation of oxygen isotopes in the reaction $^{18}\text{O} + ^{181}\text{Ta}$ have been measured at projectile nucleus energy 10 A·MeV on the high-resolution magnetic spectrometer MAVR. Theoretical analysis of product yields has been performed in the finite-range distorted-wave Born approximation formalism using the FRESKO code under the assumption of sequential neutron transfer mechanism. The results of calculations are in good agreement with experimental data.

1. Introduction

One of the major challenges in both experimental and theoretical nuclear physics is production and investigation of the properties of nuclei with extreme neutron-to-proton ratios. These nuclei are of considerable interest in connection with the question of the limits of nuclear stability, *i.e.*, the location of the neutron and proton drip-lines in the nuclear chart. At present, the neutron drip-line has been identified experimentally only up to oxygen isotopes. An interesting phenomenon is that the heaviest bound oxygen isotope is ^{24}O ($N = 16$), whereas at least ^{31}F is bound ($N = 22$), *i.e.*, the neutron drip-line extends considerably for fluorine isotopes compared to oxygen isotopes. This phenomenon has been called oxygen anomaly [1].

Currently, there are two main methods of production of light neutron-rich nuclei. The first is the use of reactions of projectile fragmentation. This method is quite efficient, but the isotope production cross sections fall substantially when moving away from the line of stability. The second method is multinucleon transfer reactions. Its advantage is the low excitation energy of the formed reaction products leading to their higher survival probability. The choice of optimal reactions for production of neutron-rich nuclei is extremely important.

In addition, experimental results in this field may provide the possibility of testing different theoretical models and extracting information on nucleon transfer mechanisms (*e.g.*, sequential



Content from this work may be used under the terms of the [Creative Commons Attribution 3.0 licence](https://creativecommons.org/licenses/by/3.0/). Any further distribution of this work must maintain attribution to the author(s) and the title of the work, journal citation and DOI.

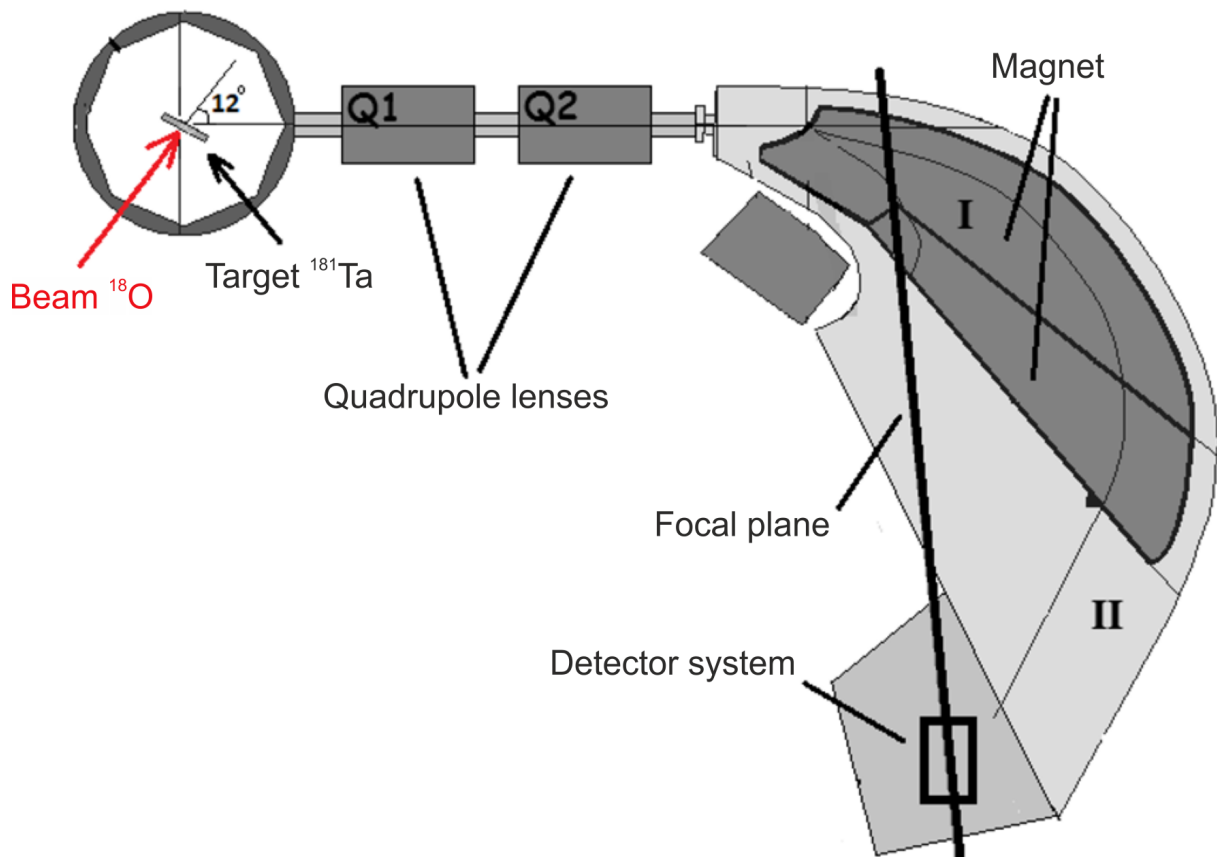


Figure 1. Scheme of experiment on the high-resolution magnetic spectrometer MAVR.

or cluster transfer). For instance, recently, cross sections and corresponding momentum distributions were measured for the first time at zero degree for the production of exotic nuclei, including neutron-rich oxygen isotopes, in the reaction of $^{18}\text{O} + ^{238}\text{U}$ at 8.5 A·MeV [2]. Comparisons of experimental results with calculations based on deep-inelastic reaction models indicated that zero degree was a scattering angle at which the differential reaction cross section for production of exotic nuclei was at its maximum.

In this work, we performed measurements of differential cross sections for the formation of oxygen isotopes the reaction $^{18}\text{O} + ^{181}\text{Ta}$ at 10 A·MeV and carried out theoretical analysis of product yields in the framework of the finite-range distorted-wave Born approximation (FR-DWBA) using the FRESCO code [3].

2. Experiment

The experiment was carried out with the beam of ^{18}O ions at energy 10 A·MeV accelerated by the U400 cyclotron, Flerov Laboratory of Nuclear Reactions (FLNR), Joint Institute for Nuclear Research (JINR). The intensity of the beam was 100 nA. The scheme of the experiment is presented in figure 1. The beam was incident on a ^{181}Ta target of thickness 4 μm . The measurements were carried out at angle $\theta_{\text{setup}} = 12^\circ$ with respect to the beam axis in the laboratory system. After leaving the target, reaction products were separated and detected by the high-resolution magnetic spectrometer MAVR [4]. The main parameters of the spectrometer are given in table 1.

The doublet of the quadrupole lenses Q1–Q2 focused isotopes of interest on the entrance

Table 1. Main parameters of the spectrometer MAVR

Interpole distance for the first magnet (mm)	47
Interpole distance for the second magnet (mm)	30
Maximum magnetic rigidity $B\rho$ (T·m)	1.5
Focal-plane angle (deg)	38–40
Focal-plane length (m)	1.9
Momentum resolution $\Delta p/p$	$1 \cdot 10^{-4}$
Energy resolution $\Delta E/E$	$5 \cdot 10^{-4}$
Charge resolution $\Delta Z/Z$	$1.7 \cdot 10^{-2}$
Mean radius of particle trajectory R (m)	1.25
Solid-angle acceptance (msr)	up to 30
Total particle bending angle in the spectrometer (deg)	111

to the magnet, which allowed us to increase the covered solid angle of the spectrometer. The calibration of the solid angle of the MAVR setup was carried out by measuring the ^{18}O nuclei, elastically scattered from the target, in the focal plane of the MAVR spectrometer.

Since the measurements were carried out at the angle $\theta_{\text{setup}} = 12^\circ$ which was significantly lower than the grazing angle $\theta_{\text{gr}} \approx 28^\circ$ for this reaction, the elastic scattering cross section was calculated by the Rutherford formula

$$\frac{d\sigma_{\text{R}}}{d\Omega}(\theta_{\text{setup}}) = \left(\frac{Z_1 Z_2 e^2}{4E} \right)^2 \frac{1}{\sin^4(\theta_{\text{setup}}/2)}, \quad (1)$$

and the solid angle covered by the setup was estimated by expression

$$\Omega_{\text{setup}} = \frac{N_{\text{els}}}{N_{\text{beam}} n_{\text{targ}}} \left[\frac{d\sigma_{\text{R}}}{d\Omega}(\theta_{\text{setup}}) \right]^{-1}, \quad (2)$$

where N_{els} is the number of the registered events for elastic scattering of the ^{18}O beam nuclei on the tantalum target, N_{beam} is the number of beam particles registered on the target, and n_{targ} is the number of target nuclei per unit area. The solid angle of the setup determined this way was $\Omega_{\text{setup}} = 1.5$ msr.

Registration and identification of reaction products in the focal plane of the spectrometer was carried out by a detector system consisting of two silicon telescopes located 25 cm apart from each other. The first telescope consisted of dE -detector (50- μm thick) and E -detector (1-mm thick); the thickness of the detectors of the second telescope was 100 μm and 1 mm for dE - and E -detectors, respectively. The thickness of the detectors was chosen from the condition of optimal resolution of oxygen isotopes. Figure 2 shows the two-dimensional identification matrices $dE \cdot E$ for the isotopes under study. It can be seen that we achieved good resolution for oxygen isotopes with mass numbers $A = 16, 17, 19, 20, 21, 22$.

To obtain the values of differential cross sections, the magnetic field of the MAVR setup was varied. The yield distribution P for each isotope was determined as the ratio of the number k_B of registered reaction events for a particular value of the magnetic field B to the linear size of the detector (2 cm) expressed in units of magnetic rigidity $\Delta(B\rho)$,

$$P(B\rho) = \frac{k_B}{\Delta(B\rho)}. \quad (3)$$

Function $P(B\rho)$ was fitted by a Gaussian and integrated over the magnetic rigidity to obtain the total isotope yield N_{isot} . The differential cross section was calculated as

$$\frac{d\sigma}{d\Omega}(\theta_{\text{setup}}) = \frac{N_{\text{isot}}}{N_{\text{beam}} n_{\text{targ}} \Omega_{\text{setup}}}. \quad (4)$$

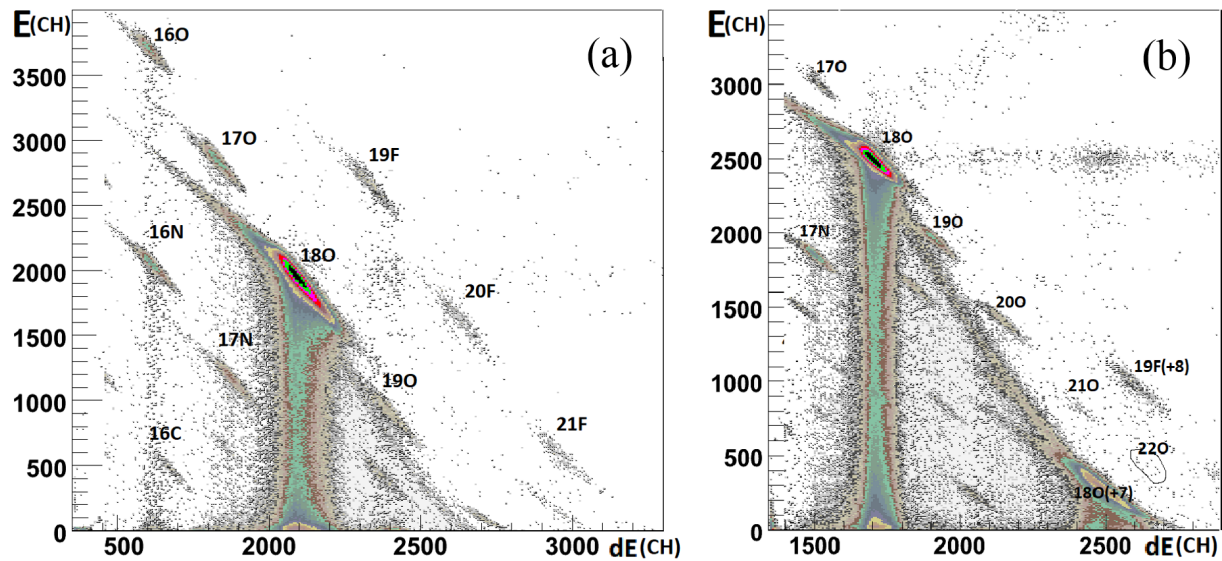


Figure 2. Identification matrices $dE \cdot E$ obtained in the focal plane of the MAVR spectrometer: (a) for neutron-deficient products with the magnetic rigidity lower than that of the beam, $B\rho < B\rho_b$; (b) for neutron-rich products with the magnetic rigidity greater than that of the beam, $B\rho > B\rho_b$.

The obtained values of the differential cross sections for the formation of oxygen isotopes in the reaction $^{18}\text{O} + ^{181}\text{Ta}$ are listed in table 2. Given uncertainties correspond to fitting uncertainties for isotope yield distributions.

Table 2. Differential cross sections for the formation of oxygen isotopes in the reaction $^{18}\text{O} + ^{181}\text{Ta}$ at $\theta_{\text{setup}} = 12^\circ$.

Isotope	^{19}O	^{20}O	^{21}O	^{22}O
$d\sigma/d\Omega$ (mb/sr)	0.309 ± 0.069	0.048 ± 0.011	0.0050 ± 0.0012	0.0010 ± 0.0002

3. Theoretical analysis

Theoretical analysis of the neutron transfer channels in the reaction $^{18}\text{O} + ^{181}\text{Ta}$ was performed in the framework of the FR-DWBA approach using the FRESCO code [3].

The values of the quadrupole deformation parameter β_2 obtained from the experimental values of quadrupole moments [5] and theoretical calculations in the finite-range liquid-drop model (FRLDM2012) [6] show that the ^{181}Ta nucleus is deformed (probably, due to the unpaired proton). In our calculations, we used the value of the quadrupole deformation parameter $\beta_2 = 0.25$ [6], spin-parity $J(\pi) = 7/2^+$, and the neutron separation energy 7.58 MeV taken from the NRV web knowledge base on low-energy nuclear physics [7, 8].

Neutron levels obtained in the model of spherical (^{18}O , ^{181}Ta) and deformed (^{181}Ta) nucleus are shown in figure 3. In the spherical ^{18}O nucleus [figure 3(a)], there are levels $2s_{1/2}$ and $1d_{5/2}$ that are free for neutron occupation. In the process of interaction, external neutrons of the deformed ^{181}Ta nucleus [figure 3(c)] may be transferred to the ^{18}O nucleus with significant probability, especially from levels with energies -7.5 MeV to -9 MeV because their energy is the closest to the energy of the free level $2s_{1/2}$ of the ^{18}O nucleus. This can lead to the transfer of up

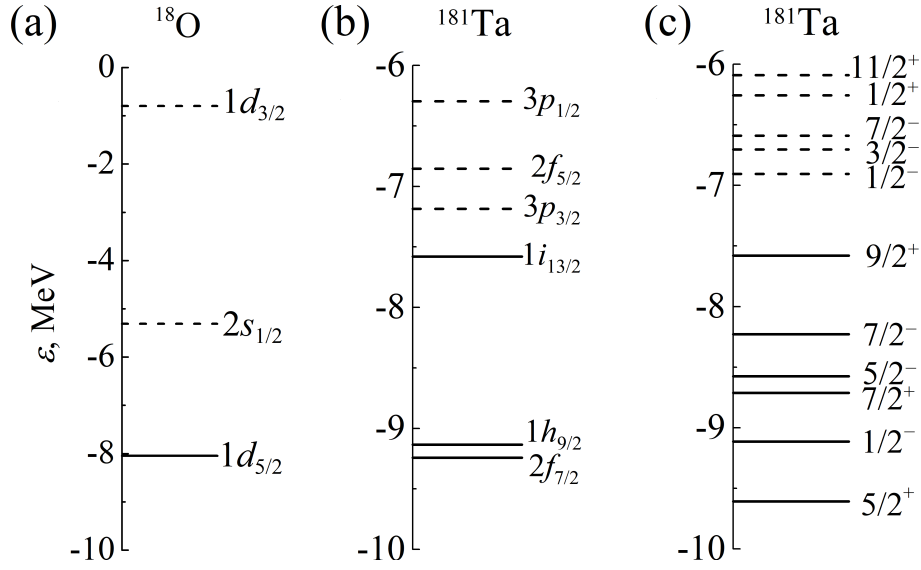


Figure 3. Upper neutron levels in the model of spherical nucleus ^{18}O (a), spherical (b) and deformed (c) nucleus ^{181}Ta .

to 10 neutrons from the target nucleus to the projectile. Due to the close location of the above-mentioned neutron levels of the deformed target nucleus, neutron transfer from these levels may be assumed equally probable. Such an approach will not lead to a fundamental difference in cross section calculations, but will greatly simplify the problem. Therefore, to calculate neutron transfer cross sections, the model of a spherical target nucleus was used, according to which there are 8 neutrons on the uppermost level $1i_{13/2}$ of the ^{181}Ta nucleus [figure 3(b)].

For an accurate quantum description of the relative motion of nuclei in the entrance and exit reaction channels, we used the Woods–Saxon optical potential with the phenomenological Akyüz–Winther parameters [9]. In the course of calculations, the depth of the imaginary part of the optical potential was varied to satisfactorily describe the experimental data. The used values of parameters are given in table 3. For all potentials, the value of the radius parameter of the Coulomb potential was chosen to be $r_C = 1.3$ fm.

Table 3. Parameters of the optical potential used for description of the relative motion of nuclei in the entrance ($^{18}\text{O} + ^{181}\text{Ta}$) and exit reaction channels.

Reaction channel	V_0 (MeV)	r_0 (fm)	a_0 (fm)	W_0 (MeV)	r_W (fm)	a_W (fm)
$^{18}\text{O} + ^{181}\text{Ta}$	63.519	1.178	0.660	16.88	1.178	0.660
$^{19}\text{O} + ^{180}\text{Ta}$	63.457	1.178	0.661	6.864	1.178	0.661
$^{20}\text{O} + ^{179}\text{Ta}$	63.457	1.178	0.661	0.902	1.178	0.661
$^{21}\text{O} + ^{178}\text{Ta}$	63.574	1.178	0.664	0.909	1.178	0.664
$^{22}\text{O} + ^{177}\text{Ta}$	63.574	1.178	0.664	0.909	1.178	0.664

The distorted waves were calculated using the potentials of the entrance and exit channels, while the reaction mechanism was determined by the wave function of the transferred neutron. The basis of the DWBA approach is calculation of the transfer amplitude

$$T_{\text{prior}} = \int dR_\alpha dR_\beta \chi_\beta^{(-)}(R_\beta) * I_{\beta\alpha}(R_\beta, R_\alpha) \chi_\alpha^{(+)}(R_\alpha), \quad (5)$$

$$I_{\beta\alpha}(R_\beta, R_\alpha) = (\phi_a\phi_B|V_{vb} + U_{ab} - U_\alpha|\phi_A\phi_b). \quad (6)$$

The internal wave functions for the initial ($\phi_A\phi_b$) and final ($\phi_a\phi_B$) nuclei play an important role in determining the transfer amplitude. To determine the internal wave functions, it is necessary to know the spin-parities J^π for the state of the final nucleus and for the “composite” nucleus, the angular momentum l of the transferred particle relative to the “core” of the nucleus, and the number of nodes N of the radial wave function.

The internal wave function with the given quantum numbers was found by varying the depth of the Woods–Saxon potential with a fixed “geometry” (radius $r_0^{\text{WS}} = 1.347$ fm, $r_0^{\text{SO}} = 1.131$ fm, and diffuseness $a^{\text{WS}} = a^{\text{SO}} = 0.7$ fm) until we achieved equality between the separation energy of the particle and the energy of the corresponding particle level taken with the opposite sign. The used spectroscopic amplitudes for sequential neutron transfer are given in table 4. They were adjustable calculation parameters.

Table 4. Spectroscopic amplitudes for neutron transfer channels.

Overlap	Spectroscopic amplitude	Overlap	Spectroscopic amplitude
$\langle^{18}\text{O} ^{19}\text{O}\rangle_{\text{g.s.}}$	0.45	$\langle^{181}\text{Ta} ^{180}\text{Ta}\rangle_{\text{g.s.}}$	0.45
$\langle^{19}\text{O} ^{20}\text{O}\rangle_{\text{g.s.}}$	1.80	$\langle^{180}\text{Ta} ^{179}\text{Ta}\rangle_{\text{g.s.}}$	1.80
$\langle^{20}\text{O} ^{21}\text{O}\rangle_{\text{g.s.}}$	1.32	$\langle^{179}\text{Ta} ^{178}\text{Ta}\rangle_{\text{g.s.}}$	1.32
$\langle^{21}\text{O} ^{22}\text{O}\rangle_{\text{g.s.}}$	1.60	$\langle^{178}\text{Ta} ^{177}\text{Ta}\rangle_{\text{g.s.}}$	1.60

Figure 4 shows the comparison of theoretical calculations with the experimental differential cross sections for neutron transfer channels $^{181}\text{Ta}(^{18}\text{O}, ^{19}\text{O})^{180}\text{Ta}$, $^{181}\text{Ta}(^{18}\text{O}, ^{20}\text{O})^{179}\text{Ta}$, $^{181}\text{Ta}(^{18}\text{O}, ^{21}\text{O})^{178}\text{Ta}$, $^{181}\text{Ta}(^{18}\text{O}, ^{22}\text{O})^{177}\text{Ta}$. It can be seen that all theoretically calculated differential cross sections are consistent with the presented experimental data. The peak near the grazing angle for the $^{181}\text{Ta}(^{18}\text{O}, ^{19}\text{O})^{180}\text{Ta}$ channel is similar to the peak observed in [10] for the two-neutron transfer channel $^{94}\text{Mo}(^{18}\text{O}, ^{16}\text{O})^{96}\text{Mo}$. This behavior of the angular distribution may explained within the classical approach. Each scattering angle is associated with a classical orbit and an impact parameter. The cross section is low at low angles (large impact parameters) and falls again at large angles due to absorption at low impact parameters. In [11], the angular distributions for the reaction $^{18}\text{O} + ^{208}\text{Pb}$ also had a bell-shaped form with a peak at the angle close to the grazing angle. Similar peaks were obtained by us in calculations of the differential cross sections for neutron transfer in the $^{18}\text{O} + ^{181}\text{Ta}$ reaction in the framework of the DWBA approach.

4. Conclusions

Using the MAVR setup, differential cross sections for the formation of oxygen isotopes in the reaction $^{18}\text{O} + ^{181}\text{Ta}$ were measured at projectile nucleus energy 10 A-MeV and laboratory angle 12° . The experimental method provided the possibility of separation of reaction products with high resolution on charge, mass, and energy. Theoretical analysis was carried out in the framework of the FR-DWBA approach using the FRESKO code under the assumption of sequential neutron transfer mechanism. Good agreement of the results of calculations with experimental data was obtained. It was shown that the MAVR setup may be used for production of neutron-rich isotopes of light nuclei in multinucleon transfer reactions.

Acknowledgments

We express our gratitude to V V Samarin for fruitful discussions. The work was supported by the Russian Science Foundation Grant No 17-12-01170 and by the Ministry of Education and Science of the Republic of Kazakhstan Grant No 303/29-03-2018.

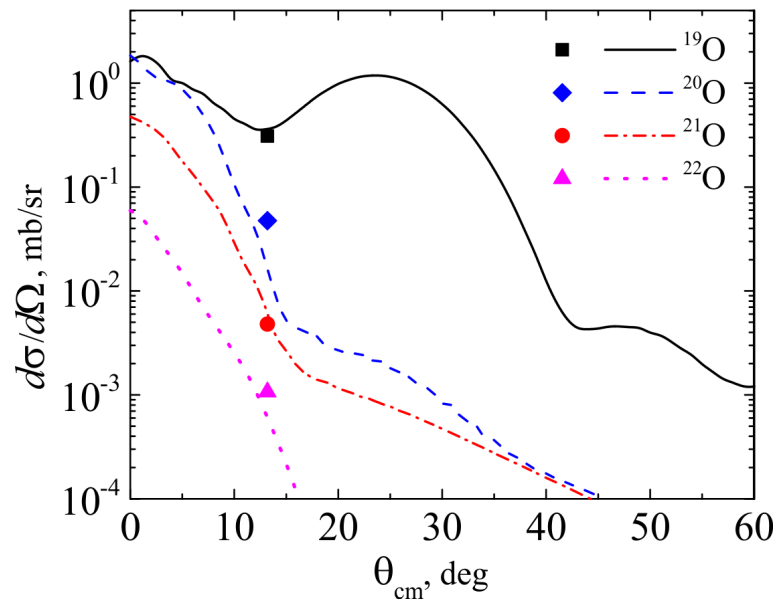


Figure 4. Differential cross sections for neutron transfer channels in the reaction $^{18}\text{O} + ^{181}\text{Ta}$ at energy 10 A-MeV with formation of reaction products $^{19-22}\text{O}$. Symbols are experimental data, lines are results of calculations in the framework of the FR-DWBA approach using the FRESKO code [3].

References

- [1] Otsuka T *et al* 2010 Three-body forces and the limit of oxygen isotopes *Phys. Rev. Lett.* **105** 032501
- [2] Stefan I *et al* 2018 Neutron-rich nuclei produced at zero degrees in damped collisions induced by a beam of ^{18}O on a ^{238}U target *Phys. Lett. B* **779** 456–459
- [3] Thompson I J 1988 Coupled reaction channels calculations in nuclear physics *Comp. Phys. Rep.* **7** 167–212; <http://www.fresco.org.uk>
- [4] Zernyshkin V A *et al* 2018 Charged particle trajectories in the MAVR high-resolution magnetic spectrometer *Phys. Part. Nucl. Lett.* **15** 531–536
- [5] Centre for Photonuclear Experiments Data (Skobeltsyn Institute of Nuclear Physics, Lomonosov Moscow State University). <http://cdfc.sinp.msu.ru/services/radchart/radmain.html>
- [6] Möller P *et al* 2016 Nuclear ground-state masses and deformations: FRDM(2012) *At. Data Nucl. Data Tables* **109–110** 1–204
- [7] NRV web knowledge base on low-energy nuclear physics. <http://nrw.jinr.ru/>
- [8] Karpov A V *et al* 2017 NRV web knowledge base on low-energy nuclear physics *Nucl. Instrum. Methods Phys. Res., Sect. A* **859** 112–124
- [9] Winther A 1994 Grazing reactions in collisions between heavy nuclei *Nucl. Phys. A* **572** 191–235
- [10] Chasman C *et al* 1972 (O18, O16) reaction on Mo isotopes at energies above the Coulomb barrier *Phys. Rev. Lett.* **28** 843–846
- [11] Sonika B J Roy *et al* 2015 *Phys. Rev. C* **92** 024603